SARS-CoV-2 transmission dynamics in South Africa and epidemiological characteristics of the Omicron variant

Wan Yang[1] and Jeffrey Shaman[2]

[1]Department of Epidemiology, [2]Department of Environmental Health Sciences, Mailman School of Public Health, Columbia University, New York, NY, USA

Correspondence to: wy2202@cumc.columbia.edu

Abstract

Within days of first detection, Omicron SARS-CoV-2 variant case numbers grew exponentially and spread globally. To better understand variant epidemiological characteristics, we utilize a model-inference system to reconstruct SARS-CoV-2 transmission dynamics in South Africa and decompose novel variant transmissibility and immune erosion. Accounting for under-detection of infection, infection seasonality, nonpharmaceutical interventions, and vaccination, we estimate that the majority of South Africans had been infected by SARS-CoV-2 before the Omicron wave. Based on findings for Gauteng province, Omicron is estimated 100.3% (95% CI: 74.8 - 140.4%) more transmissible than the ancestral SARS-CoV-2 and 36.5% (95% CI: 20.9 - 60.1%) more transmissible than Delta; in addition, Omicron erodes 63.7% (95% CI: 52.9 - 73.9%) of the population immunity, accumulated from prior infections and vaccination, in Gauteng.

Main text

In late November, 2021, South African scientists and public health officials reported a new SARS-CoV-2 variant, subsequently named Omicron.[1] Within days, SARS-CoV-2 cases due to Omicron increased dramatically in several provinces in South Africa,[2] despite substantial prior infection of the population during previous pandemic waves, including a large, recent Delta wave. Concurrently, Omicron was detected in an increasing number of countries (89, as of 12/17/21; GISAID data[3]) and appeared to spread with unprecedented speed in several European countries.[4,5] Multiple laboratory studies have reported large reductions (~20-40x) in neutralizing ability of convalescent sera and vaccinee sera against Omicron, suggesting this variant is able to erode components of adaptive immunity.[6-9] In addition, preliminary *in vitro* and/or *ex vivo* studies indicate that Omicron replicates faster within host than the Delta SARS-CoV-2 variant,[8,10] which has been the predominant variant since mid 2021. Together, this early epidemiological and laboratory evidence points to both immune erosion and increased transmissibility of Omicron. However, the relative importance of these two quantities remains unclear.

To better understand the epidemiological characteristics of Omicron, we utilize a model-inference system similar to one developed for study of SARS-CoV-2 variants of concern (VOCs), including the Beta variant.[11] We use this system first to reconstruct SARS-CoV-2 transmission

dynamics in each of the nine provinces in South Africa, accounting for under-detection of infection, infection seasonality, implemented nonpharmaceutical interventions (NPIs), and vaccination (see Methods). Overall, the model-inference system is able to fit weekly case and death data in each province (Fig 1A and Fig S1). We further validated the model-inference estimates using three independent datasets. First, we used serology data. We note that early in the pandemic serology data may reflect underlying infection rates but later, due to waning antibody titers and reinfection, likely underestimate infection. Compared to seroprevalence measures taken at multiple time points in each province, our model estimated cumulative infection rates roughly match corresponding serology measures and trends over time; as expected, model estimates were higher than serology measures taken during later months (Fig 1B). Second, compared to hospital admission data, across the nine provinces, model estimated infection numbers were well correlated with numbers of hospitalizations for all three initial pandemic waves caused by the ancestral, Beta, and Delta variants, respectively ($r > .85$, Fig 1 C-E). Third, model-estimated infection numbers were correlated with age-adjusted excess mortality for both the ancestral and Delta wave, but not the Beta wave (Fig 1C and E, vs. Fig 1D). Overall, these comparisons indicate our model-inference estimates align with underlying transmission dynamics.

Next, we use Gauteng – the province with the earliest surge of Omicron – as an example to highlight pandemic dynamics in South Africa thus far and develop key model-inference estimates (Fig 2 for Gauteng and Fig S 2-9 for each of the other eight provinces). Despite lower cases per capita than many other countries, infection numbers in South Africa were likely much higher due to under-detection. For Gauteng, the estimated infection-detection rate during the first pandemic wave was 4.31% (95% CI: 2.53 - 8.75%), and increased slightly to 5.21% (95% CI: 2.94 - 9.47%) and 5.88% (95% CI: 3.40 - 11.32%) during the Beta and Delta waves, respectively (Table S1). These estimates are in line with those reported elsewhere based on serology data (e.g., 4.74% detection rate during the first wave[12]). Accounting for under-detection (Fig 2E), we estimate that 34.99% (95% CI: 17.22 - 59.52%, Table S2) of the population in Gauteng were infected during the first wave, predominantly during winter when more conducive climate conditions and relaxed public health restrictions existed (see the estimated seasonal and mobility trends, Fig 2A).

With the emergence of Beta, another 25.91% (95% CI: 14.26 - 45.91%) of the population in Gauteng – including reinfections – is estimated to have been infected, even though the Beta wave occurred during summer under less conducive climate conditions for transmission (Fig 2A). Consistent with laboratory studies showing low neutralizing ability of convalescent sera against Beta,[13,14] the model-inference system estimates a large increase in population susceptibility with the surge of Beta (Fig 2D). In addition to this immune erosion, an increase in

transmissibility is also evident for Beta, after accounting for concurrent NPIs and infection seasonality (Fig 2C). Notably, in contrast to the large fluctuation of the time-varying effective reproduction number over time (R_t, Fig 2B), the transmissibility estimates are more stable and reflect changes in variant-specific properties. Further, consistent with in-depth epidemiological findings,[15] the estimated overall infection-fatality risk was higher for Beta than Ancestral SARS-CoV-2 (0.16% [95% CI: 0.09 - 0.28%] vs. 0.09% [95% CI: 0.05 - 0.18%], Fig 2F and Table S3; n.b. these estimates are based on documented COVID-19 deaths and are likely underestimates).

With the introduction of Delta, a third pandemic wave occurred in Gauteng during the 2021 winter. The model-inference system estimates a 53.19% (95% CI: 27.61 - 91.87%) attack rate by Delta, despite the large number of infections during the previous two waves. This large attack rate was possible, due to the high transmissibility of Delta, as reported in multiple studies,[16-20] the more conducive winter transmission conditions (Fig 2A), and the immune erosion from Delta relative to both the ancestral and Beta variants. Consistent with this finding, and in particular the estimated immune erosion, studies have reported a 27.5% reinfection rate during the Delta pandemic wave in Delhi, India[21] and reduced ability of sera from Beta-infection recoverees to neutralize Delta.[22,23]

Due to these large pandemic waves, prior to the detection of Omicron in Gauteng, estimated cumulative infection numbers surpassed the population size (Fig 3B), indicating the large majority of the population had been infected and some more than once. With the rise of Omicron, the model-inference system estimates a very large increase in population susceptibility (Fig 2D), as well as an increase in transmissibility (Fig 2C); however, unlike previous waves, the Omicron wave progresses much more quickly, peaking 2-3 weeks after initiating marked exponential growth. These estimates suggest that several additional factors may have also contributed to the observed dynamics, including changes to the infection-detection rate (Fig 2E), a summer seasonality increasingly suppressing transmission as the wave progresses (Fig 2A), as well as a slight change in population mobility suggesting potential behavior changes (Fig 2A).

Across all nine provinces in South Africa, the pandemic timing and intensity varied (Fig 3 A-C). In addition to Gauteng, high cumulative infection rates during the first three pandemic waves are also estimated for Western Cape and Northern Cape (Fig 1 C-E, Fig 3B and Table S2). Overall, all nine provinces likely experienced three large pandemic waves prior to the growth of Omicron; estimated average cumulative infections ranged from 58% of the population in Limpopo to 126% in Northern Cape (Fig 3B).

Combining these model-inference estimates during each wave in each province, we estimate that Beta eroded immunity among 72.1% (95% CI: 52.8 - 88.6%) of individuals with prior ancestral SARS-CoV-2 infection and was 38.5% (95% CI: 16.2 – 56.0%) more transmissible than the ancestral SARS-CoV-2. These estimates for Beta are consistent across the nine provinces (Fig 3D, 1st column), as well as with our previous estimates using national data for South Africa.[11] In comparison, estimates for Delta vary across the nine provinces (Fig 3D, 2nd column), given the more diverse population immune landscape among provinces after two pandemic waves. Overall, we estimate that Delta eroded 32.5% (95% CI: 0 – 60.9%) of prior immunity (gained from infection by ancestral SARS-CoV-2 and/or Beta, and/or vaccination) and was 38.3% (95% CI: 21.2 - 58.5%) more transmissible than the ancestral SARS-CoV-2.

For Omicron, based on three provinces with the earliest surges (i.e., Gauteng, North West, and Western Cape), we estimate that this variant erodes 55.0% (95% CI: 40.9 - 71.4%) of immunity due to all prior infections and vaccination. In addition, it is 92.2% (95% CI: 70.2 - 128.5%) more transmissible than the ancestral SARS-CoV-2. Based on estimates for Gauteng alone, Omicron is 100.3% (95% CI: 74.8 - 140.4%) more transmissible than the ancestral SARS-CoV-2, and 36.5% (95% CI: 20.9 - 60.1%) more transmissible than Delta; in addition, it erodes 63.7% (95% CI: 52.9 - 73.9%) of the population immunity, accumulated from prior infections and vaccination, in Gauteng.

Using a comprehensive model-inference system, we have reconstructed the pandemic dynamics in each of the nine provinces in South Africa. Estimated underlying infection rates (Fig 1B-E) and key parameters (e.g. infection-detection rate and infection-fatality risk) are in line with independent epidemiological data and investigations. These detailed model-inference estimates thus allow assessment of both the transmissibility and immune erosion potential of Omicron, and help contextualization and interpretation of Omicron transmission dynamics in places outside South Africa. We show that, prior to the rise of Omicron, in Gauteng, the large majority of population had been infected by one or more SARS-CoV-2 variants (including the ancestral virus, Beta, and Delta), suggesting a high rate of immune erosion by Omicron versus most, if not all, prior SARS-CoV-2 variants and vaccines. Interestingly, preliminary laboratory data show that only 1 of 8 Beta, 1 of 7 Delta, and 0 of 10 Alpha convalescent sera had 50% neutralization titers (IC50) >1:16 for Omicron.[9] Combining these laboratory data with our estimates of infection rates suggests 11% of the population would have retained immunity against Omicron from prior Beta and Delta infection (i.e., 1/8 × 25.9% attack rate by Beta + 1/7 × 53.2% attack rate by Delta). However, studies have reported retained neutralizing ability against Omicron among recoverees additionally vaccinated with 2 doses of vaccine.[7,9] Assuming an 80% probability of prior infection among the ~25% of Gauteng who received at least 1 vaccine dose (by the end of Nov 2021), another 20% of population would have gained

immunity against Omicron from infection plus vaccination. In combination, this simple conversion suggests the remaining ~70% of the population would be susceptible to Omicron, similar to our model estimates (Fig 2D). Given the challenge of jointly estimating population susceptibility (needed for estimating both prior immunity and immune erosion) and transmissibility, the consistency of our population susceptibility estimates with available laboratory evidence indicates that our estimates of transmissibility are also sensible.

Population susceptibility may differ across locations depending upon prior exposure to different SARS-CoV-2 variants and vaccination uptake. However, similar calculations can be made in other countries and regions, given prior infection and vaccination rates, in order to gauge local susceptibility. In combination with the increased transmissibility estimated here and other location conditions (e.g., infection seasonality and implementation of NPIs), modeling can then be used to better anticipate the course of the Omicron wave. Nonetheless, the ability of Omicron to spread with unprecedented pace in a heavily infected and partially vaccinated population should serve as an alert for prompt public health response. More fundamentally, it is yet another indication of the need for a global effort for increased vaccination, recurrent boosting, and the development and distribution of effective and safe therapeutics for all populations around the world.

METHODS

Data sources and processing

We used reported COVID-19 case and mortality data to capture transmission dynamics, weather data to estimate infection seasonality, mobility data to represent concurrent NPIs, and vaccination data to account for changes in population susceptibility due to vaccination in the model-inference system. Provincial level COVID-19 case, mortality, and vaccination data were sourced from the Coronavirus COVID-19 (2019-nCoV) Data Repository for South Africa (COVID19ZA).[24] Hourly surface station temperature and relative humidity came from the Integrated Surface Dataset (ISD) maintained by the National Oceanic and Atmospheric Administration (NOAA) and are accessible using the "stationaRy" R package.[25,26] We computed specific humidity using temperature and relative humidity per the Clausius-Clapeyron equation.[27] We then aggregated these data for all weather stations in each province with measurements since 2000 and calculated the average for each week of the year during 2000-2020.

Mobility data were derived from Google Community Mobility Reports;[28] we aggregated all business-related categories (i.e., retail and recreational, transit stations, and workplaces) in all locations in each province to weekly intervals. For vaccination, provincial vaccination data from the COVID19ZA data repository recorded the total number of vaccine doses administered over

time; to obtain a breakdown for numbers of partial (1 dose of mRNA vaccine) and full vaccinations (1 dose of Janssen vaccine or 2 doses of mRNA vaccine), separately, we used national vaccination data for South Africa from Our World in Data[29,30] to apportion the doses each day. In addition, cumulative case data suggested 18,586 new cases on Nov 23, 2021, whereas the South Africa Department of Health reported 868.[31] Thus, for Nov 23, 2021, we used linear interpolation to fill in estimates for each province on that day and then scaled the estimates such that they sum to 868.

Model-inference system

The model-inference system is based on our previous work estimating changes in transmissibility and immune erosion for SARS-CoV-2 VOCs including Alpha, Beta, Gamma, and Delta.[11,32] Below we describe each component.

Epidemic model

The epidemic model follows an SEIRSV (susceptible-exposed-infectious-recovered-susceptible-vaccination) construct per Eqn 1:

$$\begin{cases} \dfrac{dS}{dt} = \dfrac{R}{L_t} - \dfrac{b_t e_t m_t \beta_t IS}{N} - \varepsilon - v_{1,t} - v_{2,t} \\ \dfrac{dE}{dt} = \dfrac{b_t e_t m_t \beta_t IS}{N} - \dfrac{E}{Z_t} + \varepsilon \\ \dfrac{dI}{dt} = \dfrac{E}{Z_t} - \dfrac{I}{D_t} \\ \dfrac{dR}{dt} = \dfrac{I}{D_t} - \dfrac{R}{L_t} + v_{1,t} + v_{2,t} \end{cases}$$

where S, E, I, R are the number of susceptible, exposed (but not yet infectious), infectious, and recovered/immune/deceased individuals; N is the population size; and ε is the number of travel-imported infections. In addition, the model includes the following key components:

1) Virus-specific properties, including the time-varying variant-specific transmission rate β_t, latency period Z_t, infectious period D_t, and immunity period L_t. Note all parameters are estimated for each week (t) as described below.
2) The impact of NPIs. Specifically, we use relative population mobility (see data above) to adjust the transmission rate via the term m_t, as the overall impact of NPIs (e.g., reduction in the time-varying effective reproduction number R_t) has been reported to be highly correlated with population mobility during the COVID-19 pandemic.[33-35] To further account for potential changes in effectiveness, the model additionally includes a parameter, e_t, to scale NPI effectiveness.

3) The impact of vaccination, via the terms $v_{1,t}$ and $v_{2,t}$. Specifically, $v_{1,t}$ is the number of individuals successfully immunized after the first dose of vaccine and is computed using vaccination data and vaccine effectiveness (VE) for 1st dose; and $v_{2,t}$ is the additional number of individuals successfully immunized after the second vaccine dose (i.e., excluding those successfully immunized after the first dose). In South Africa, around two-thirds of vaccines administered during our study period were the mRNA BioNTech/Pfizer vaccine and one-third the Janssen vaccine.[36] We thus set VE to 20%/85% (partial/full vaccination) for Beta, 35%/75% for Delta, and 10%/35% for Omicron based on reported VE estimates.[37-39]

4) Infection seasonality, computed using temperature and specific humidity data as described previously (see supplemental material of Yang and Shaman[11]). Briefly, we estimated the relative seasonal trend (b_t) using a model representing the dependency of the survival of respiratory viruses including SARS-CoV-2 to temperature and humidity.[40,41] As shown in Fig 2A, b_t estimates over the year averaged to 1 such that weeks with b_t >1 (e.g. during the winter) are more conducive to SARS-CoV-2 transmission whereas weeks with b_t <1 (e.g. during the summer) have less favorable climate conditions for transmission. The estimated relative seasonal trend, b_t, is used to adjust the relative transmission rate at time t in Eqn 1.

Observation model to account for under-detection and delay

Using the model-simulated number of infections occurring each day, we further computed the number of cases and deaths each week to match with the observations, as done in Yang et al.[42] Briefly, we include 1) a time-lag from infectiousness to detection (i.e., an infection being diagnosed as a case), drawn from a gamma distribution with a mean of $T_{d,mean}$ days and a standard deviation of $T_{d,\,sd}$ days, to account for delays in detection (Table S4); 2) an infection-detection rate (r_t), i.e. the fraction of infections (including subclinical or asymptomatic infections) reported as cases, to account for under-detection; 3) a time-lag from infectiousness to death, drawn from a gamma distribution with a mean of 13-15 days and a standard deviation of 10 days; and 4) an infection-fatality risk (IFR_t). To compute the model-simulated number of new cases each week, we multiplied the model-simulated number of new infections per day by the infection-detection rate, and further distributed these simulated cases in time per the distribution of time-from-infectiousness-to-detection. Similarly, to compute the model-simulated deaths per week and account for delays in time to death, we multiplied the simulated-infections by the IFR and then distributed these simulated deaths in time per the distribution of time-from-infectious-to-death. We then aggregated these daily numbers to weekly totals to match with the weekly case and mortality data for model-inference. For each week, the infection-detection rate (r_t), the infection-fatality risk (IFR_t)., and the two time-to-detection parameters ($T_{d,mean}$ and $T_{d,\,sd}$) were estimated along with other parameters (see below).

Model inference and parameter estimation

The inference system uses the ensemble adjustment Kalman filter, EAKF,[43] a Bayesian statistical method, to estimate model state variables (i.e., *S*, *E*, *I*, *R* from Eqn 1) and parameters (i.e., β_t, Z_t, D_t, L_t, e_t, from Eqn 1 as well as r_t, IFR_t and other parameters from the observation model). Briefly, the EAKF uses an ensemble of model realizations (*n*=500 here), each with initial parameters and variables randomly drawn from a *prior* range (see Table S4). After model initialization, the system integrates the model ensemble forward in time for a week (per Eqn 1) to compute the prior distribution for each model state variable and parameter, as well as the model-simulated number of cases and deaths for that week. The system then combines the prior estimates with the observed case and death data for the same week to compute the posterior per Bayes' theorem.[43] During this filtering process, the system updates the posterior distribution of all model variables and parameters for each week.

Estimating changes in transmissibility and immune erosion for each variant

As in ref[11], we computed the variant-specific transmissibility (R_{TX}) as the product of the variant-specific transmission rate (β_t) and infectious period (D_t). Note that R_t, the time-varying effective reproduction number, is defined as $R_t = b_t e_t m_t \beta_t D_t S/N = b_t e_t m_t R_{TX} S/N$. To reduce uncertainty, we averaged transmissibility estimates over the period a particular variant of interest was predominant. To find these predominant periods, we first specified the approximate timing of each pandemic wave in each province based on: 1) when available, genomic surveillance data; specifically, the onsets of the Beta wave in Eastern Cape, Western Cape, KwaZulu-Natal, and Northern Cape, were separately based on the initial detection of Beta in these provinces as reported in Tegally et al;[44] the onsets of the Delta wave in each of the nine provinces, separately, were based on genomic sequencing data from the Network for Genomic Surveillance South Africa (NGS-SA);[45] and 2) when genomic data were not available, we used the week with the lowest case number between two waves. The specified calendar periods are listed in Table S5. During later waves, multiple variants could initially co-circulate before one became predominant. As a result, the estimated transmissibility tended to increase before reaching a plateau (see, e.g., Fig 2C). In addition, in a previous study of the Delta pandemic wave in India,[32] we also observed that when many had been infected, transmissibility could decrease a couple months after the peak, likely due to increased reinfections for which onward transmission may be reduced. Thus, to obtain a more variant-specific estimate, we computed the average transmissibility ($\overline{R_{TX}}$) using the weekly R_{TX} estimates over the 8-week period starting the week prior to the maximal R_{tx} during each wave; if no maximum existed (e.g. when a new variant is less transmissible), we simply averaged over the entire wave. We then

computed the change in transmissibility due to a given variant relative to the ancestral SARS-CoV-2 as $\left(\frac{\overline{R_{TX,variant}}-\overline{R_{TX,ancestral}}}{\overline{R_{TX,ancestral}}}\right)\times 100\%$.

To quantify immune erosion, similar to ref[11], we estimated changes in susceptibility over time and computed the change in immunity as ΔImm = $S_{t+1} - S_t + i_t$, where S_t is the susceptibility at time-t and i_t is the new infections occurring during each week-t. We sum over all ΔImm estimates for a particular location, during each wave, to compute the total change in immunity due to a new variant, $\Sigma\Delta Imm_v$. We then computed the level of immune erosion as the ratio of $\Sigma\Delta Imm_v$ to the model-estimated population immunity prior to the first detection of immune erosion, during each wave. That is, as opposed to having a common reference of prior immunity, here immune erosion for each variant depends on the state of the population immune landscape – i.e., combining all prior exposures and vaccinations – immediately preceding the surge of that variant.

For all provinces, model-inference was initiated the week starting March 15, 2020 and run continuously until the week starting Dec 12, 2021. To account for model stochasticity, we repeated the model-inference process 100 times for each province, each with 500 model realizations and summarized the results from all 50,000 model estimates.

Model validation using independent data

To compare model estimates with independent observations not assimilated into the model-inference system, we utilized three relevant datasets:

1) Serological survey data measuring the prevalence of SARS-CoV-2 antibodies over time. Multiple serology surveys have been conducted in different provinces of South Africa. The South African COVID-19 Modelling Consortium summarizes the findings from several of these surveys (see Fig 1A of ref [46]). We digitized all data presented in Fig 1A of ref [46] and compared these to corresponding model-estimated cumulative infection rates (computed mid-month for each corresponding month with a seroprevalence measure). Due to unknown survey methodologies and challenges adjusting for sero-reversion and reinfection, we used these data directly (i.e., without adjustment) for qualitative comparison.
2) COVID-19-related hospitalization data, from COVID19ZA.[24] We aggregated the total number of COVID-19 hospital admissions during each wave and compared these aggregates to model-estimated cumulative infection rates during the same wave. Of note, these hospitalization data were available from June 6, 2020 onwards and are thus incomplete for the first wave.

3) Age-adjusted excess mortality data from the South African Medical Research Council (SAMRC).[47] Deaths due to COVID-19 (used in the model-inference system) are undercounted. Thus, we also compared model-estimated cumulative infection rates to age-adjusted excess mortality data during each wave. Of note, excess mortality data were available from May 3, 2020 onwards and are thus incomplete for the first wave.

Data Availability: All data used in this study are publicly available as described in the "Data sources and processing" section.

Code availability: All source code and data necessary for the replication of our results and figures will be made publicly available on Github.

Acknowledgements: This study was supported by the National Institute of Allergy and Infectious Diseases (AI145883 and AI163023), the Centers for Disease Control and Prevention (CK000592), and a gift from the Morris-Singer Foundation.

Author contributions: WY designed the study (main), conducted the model analyses, interpreted results, and wrote the first draft. JS designed the study (supporting), interpreted results, and critically revised the manuscript.

Competing interests: JS and Columbia University disclose partial ownership of SK Analytics. JS discloses consulting for BNI.

References:

1 World Health Organization. Classification of Omicron (B.1.1.529): SARS-CoV-2 Variant of Concern. (2021).

2 Viana et al. *Rapid epidemic expansion of the SARS-CoV-2 Omicron variant in southern Africa*, <https://krisp.org.za/manuscripts/ZHTOWa-MEDRXIV-2021-268028v1-deOliveira.pdf> (2021).

3 Global Initiative on Sharing All Influenza Data (GISAID). *Tracking of Variants*, <https://www.gisaid.org/hcov19-variants/> (2021).

4 UK Heath Security Agency. Omicron daily overview: 17 December 2021. (2021).

5 Espenhain, L. *et al.* Epidemiological characterisation of the first 785 SARS-CoV-2 Omicron variant cases in Denmark, December 2021. *Eurosurveillance* **26**, 2101146, doi:doi:https://doi.org/10.2807/1560-7917.ES.2021.26.50.2101146 (2021).

6 Nemet, I. *et al.* Third BNT162b2 vaccination neutralization of SARS-CoV-2 Omicron infection. *medRxiv*, 2021.2012.2013.21267670, doi:10.1101/2021.12.13.21267670 (2021).

7 Cele, S. *et al.* SARS-CoV-2 Omicron has extensive but incomplete escape of Pfizer BNT162b2 elicited neutralization and requires ACE2 for infection. *medRxiv*, 2021.2012.2008.21267417, doi:10.1101/2021.12.08.21267417 (2021).
8 Garcia-Beltran, W. F. *et al.* mRNA-based COVID-19 vaccine boosters induce neutralizing immunity against SARS-CoV-2 Omicron variant. *medRxiv*, 2021.2012.2014.21267755, doi:10.1101/2021.12.14.21267755 (2021).
9 Rössler, A., Riepler, L., Bante, D., Laer, D. v. & Kimpel, J. SARS-CoV-2 B.1.1.529 variant (Omicron) evades neutralization by sera from vaccinated and convalescent individuals. *medRxiv*, 2021.2012.2008.21267491, doi:10.1101/2021.12.08.21267491 (2021).
10 Li Ka Shing Faculty of Medicine. *HKUMed finds Omicron SARS-CoV-2 can infect faster and better than Delta in human bronchus but with less severe infection in lung*, 2021).
11 Yang, W. & Shaman, J. Development of a model-inference system for estimating epidemiological characteristics of SARS-CoV-2 variants of concern. *Nature Communications* **12**, 5573, doi:https://doi.org/10.1038/s41467-021-25913-9 (2021).
12 Kleynhans, J. *et al.* SARS-CoV-2 Seroprevalence in a Rural and Urban Household Cohort during First and Second Waves of Infections, South Africa, July 2020-March 2021. *Emerg Infect Dis* **27**, 3020-3029, doi:10.3201/eid2712.211465 (2021).
13 Garcia-Beltran, W. F. *et al.* Multiple SARS-CoV-2 variants escape neutralization by vaccine-induced humoral immunity. *Cell* **184**, 2372-2383 e2379, doi:10.1016/j.cell.2021.03.013 (2021).
14 Wall, E. C. *et al.* Neutralising antibody activity against SARS-CoV-2 VOCs B.1.617.2 and B.1.351 by BNT162b2 vaccination. *Lancet*, doi:10.1016/S0140-6736(21)01290-3 (2021).
15 Abu-Raddad, L. J. *et al.* Severity, Criticality, and Fatality of the Severe Acute Respiratory Syndrome Coronavirus 2 (SARS-CoV-2) Beta Variant. *Clinical Infectious Diseases*, doi:10.1093/cid/ciab909 (2021).
16 Public Health England. *SARS-CoV-2 variants of concern and variants under investigation in England. Technical briefing 14*, <https://assets.publishing.service.gov.uk/government/uploads/system/uploads/attachment_data/file/991343/Variants_of_Concern_VOC_Technical_Briefing_14.pdf> (2021).
17 Allen, H. *et al.* Household transmission of COVID-19 cases associated with SARS-CoV-2 delta variant (B.1.617.2): national case-control study. *The Lancet regional health. Europe*, 100252, doi:10.1016/j.lanepe.2021.100252 (2021).
18 Challen, R. *et al.* Early epidemiological signatures of novel SARS-CoV-2 variants: establishment of B.1.617.2 in England. *medRxiv*, 2021.2006.2005.21258365, doi:10.1101/2021.06.05.21258365 (2021).
19 Earnest, R. *et al.* Comparative transmissibility of SARS-CoV-2 variants Delta and Alpha in New England, USA. *medRxiv*, doi:10.1101/2021.10.06.21264641 (2021).
20 Vohringer, H. S. *et al.* Genomic reconstruction of the SARS-CoV-2 epidemic in England. *Nature*, doi:10.1038/s41586-021-04069-y (2021).
21 Dhar, M. S. *et al.* Genomic characterization and epidemiology of an emerging SARS-CoV-2 variant in Delhi, India. *Science*, eabj9932, doi:10.1126/science.abj9932 (2021).
22 Liu, C. *et al.* Reduced neutralization of SARS-CoV-2 B.1.617 by vaccine and convalescent serum. *Cell* **184**, 4220-+, doi:10.1016/j.cell.2021.06.020 (2021).

23 de Oliveira, T. & Lessells, R. *Update on Delta and other variants in South Africa and other world*, <https://www.krisp.org.za/manuscripts/DeltaGammaSummary_NGS-SA_6JulV2.pdf> (2021).
24 Data Science for Social Impact Research Group at University of Pretoria. *Coronavirus COVID-19 (2019-nCoV) Data Repository for South Africa*, <https://github.com/dsfsi/covid19za> (2021).
25 Iannone, R. *Package 'stationaRy'*, <https://cran.r-project.org/web/packages/stationaRy/stationaRy.pdf> (2020).
26 Iannone, R. *stationaRy*, <https://github.com/rich-iannone/stationaRy> (2020).
27 Wallace, J. & Hobbs, P. *Atmospheric Science: An Introductory survey*. 2nd Edition edn, (Academic Press, 2006).
28 Google Inc. *Community Mobility Reports*, <https://www.google.com/covid19/mobility/> (2020).
29 *Data on COVID-19 (coronavirus) vaccinations by Our World in Data*, <https://github.com/owid/covid-19-data/tree/master/public/data/vaccinations> (2020).
30 Mathieu, E. *et al.* A global database of COVID-19 vaccinations. *Nat Hum Behav* **5**, 947-953, doi:10.1038/s41562-021-01122-8 (2021).
31 Department of Health Republic of South Africa. *Update on Covid-19 (Tuesday 23 November 2021)*, <https://sacoronavirus.co.za/2021/11/23/update-on-covid-19-tuesday-23-november-2021/> (2021).
32 Yang, W. & Shaman, J. COVID-19 pandemic dynamics in India, the SARS-CoV-2 Delta variant, and implications for vaccination. *medRxiv*, 2021.2006.2021.21259268, doi:10.1101/2021.06.21.21259268 (2021).
33 Yang, W., Shaff, J. & Shaman, J. Effectiveness of non-pharmaceutical interventions to contain COVID-19: a case study of the 2020 spring pandemic wave in New York City. *J R Soc Interface* **18**, 20200822, doi:10.1098/rsif.2020.0822 (2021).
34 Lasry, A. *et al.* Timing of Community Mitigation and Changes in Reported COVID-19 and Community Mobility - Four U.S. Metropolitan Areas, February 26-April 1, 2020. *MMWR. Morbidity and mortality weekly report* **69**, 451-457, doi:10.15585/mmwr.mm6915e2 (2020).
35 Kraemer, M. U. G. *et al.* The effect of human mobility and control measures on the COVID-19 epidemic in China. *Science* **368**, 493-497, doi:10.1126/science.abb4218 (2020).
36 Department of Health Republic of South Africa. *Latest Vaccine Statistics*, <https://sacoronavirus.co.za/latest-vaccine-statistics/> (2021).
37 Abu-Raddad, L. J., Chemaitelly, H. & Butt, A. A. Effectiveness of the BNT162b2 Covid-19 Vaccine against the B.1.1.7 and B.1.351 Variants. *New Engl J Med*, doi:10.1056/NEJMc2104974 (2021).
38 Bernal, J. L. *et al.* Effectiveness of Covid-19 Vaccines against the B.1.617.2 (Delta) Variant. *New England Journal of Medicine* **385**, 585-594, doi:10.1056/NEJMoa2108891 (2021).
39 Andrews, N. *et al.* Effectiveness of COVID-19 vaccines against the Omicron (B.1.1.529) variant of concern. *medRxiv*, 2021.2012.2014.21267615, doi:10.1101/2021.12.14.21267615 (2021).

40 Biryukov, J. *et al.* Increasing Temperature and Relative Humidity Accelerates Inactivation of SARS-CoV-2 on Surfaces. *mSphere* **5**, e00441-00420, doi:doi:10.1128/mSphere.00441-20 (2020).
41 Morris, D. H. *et al.* Mechanistic theory predicts the effects of temperature and humidity on inactivation of SARS-CoV-2 and other enveloped viruses. *Elife* **10**, doi:10.7554/eLife.65902 (2021).
42 Yang, W. *et al.* Estimating the infection-fatality risk of SARS-CoV-2 in New York City during the spring 2020 pandemic wave: a model-based analysis. *The Lancet. Infectious diseases* **21**, 203-212, doi:10.1016/S1473-3099(20)30769-6 (2021).
43 Anderson, J. L. An ensemble adjustment Kalman filter for data assimilation. *Mon. Weather Rev.* **129**, 2884-2903, doi:Doi 10.1175/1520-0493(2001)129<2884:Aeakff>2.0.Co;2 (2001).
44 Tegally, H. *et al.* Detection of a SARS-CoV-2 variant of concern in South Africa. *Nature* **592**, 438-443, doi:10.1038/s41586-021-03402-9 (2021).
45 The National Institute for Communicable Diseases (NICD) of the National Health Laboratory (NHLS) on behalf of the Network for Genomics Surveillance in South Africa (NGS-SA). *Network for Genomic Surveillance South Africa (NGS-SA) SARS-CoV-2 Sequencing Update 19 August 2021*, < https://www.nicd.ac.za/wp-content/uploads/2021/08/Update-of-SA-sequencing-data-from-GISAID-19-August-2021.pdf> (2021).
46 The South African COVID-19 Modelling Consortium. *COVID-19 modelling update: Considerations for a potential fourth wave (17 Nov 2021)*, <https://www.nicd.ac.za/wp-content/uploads/2021/11/SACMC-Fourth-wave-report-17112021-final.pdf> (2021).
47 The South African Medical Research Council (SAMRC). *Report on Weekly Deaths in South Africa*, <https://www.samrc.ac.za/reports/report-weekly-deaths-south-africa> (2021).

Fig 1. Pandemic dynamics in South Africa, model-fit and validation using independent data. (A) Pandemic dynamics in each of the nine provinces (see legend); dots depict reported weekly numbers of cases and deaths; lines show model mean estimates (in the same color). For validation, model estimated infection rates are compared to seroprevalence measures over time from multiple sero-surveys summarized in ref [1] (B), COVID-related hospitalizations (left panel) and age-adjusted excess mortality (right panel) during the Ancestral (C), Beta (D), and Delta (E) waves. Boxplots depict the estimated distribution for each province (middle bar = mean; edges = 50% CrIs) and whiskers (95% CrIs). Red dots show corresponding measurements. Correlation (*r*) between model estimated cumulative infection rate and cumulative hospitalization or age-adjusted excess mortality (C-E) for each wave is shown in each plot. *Note that hospitalization data begin from 6/6/20 and excess mortality data begin from 5/3/20 and thus are incomplete for the Ancestral wave.*

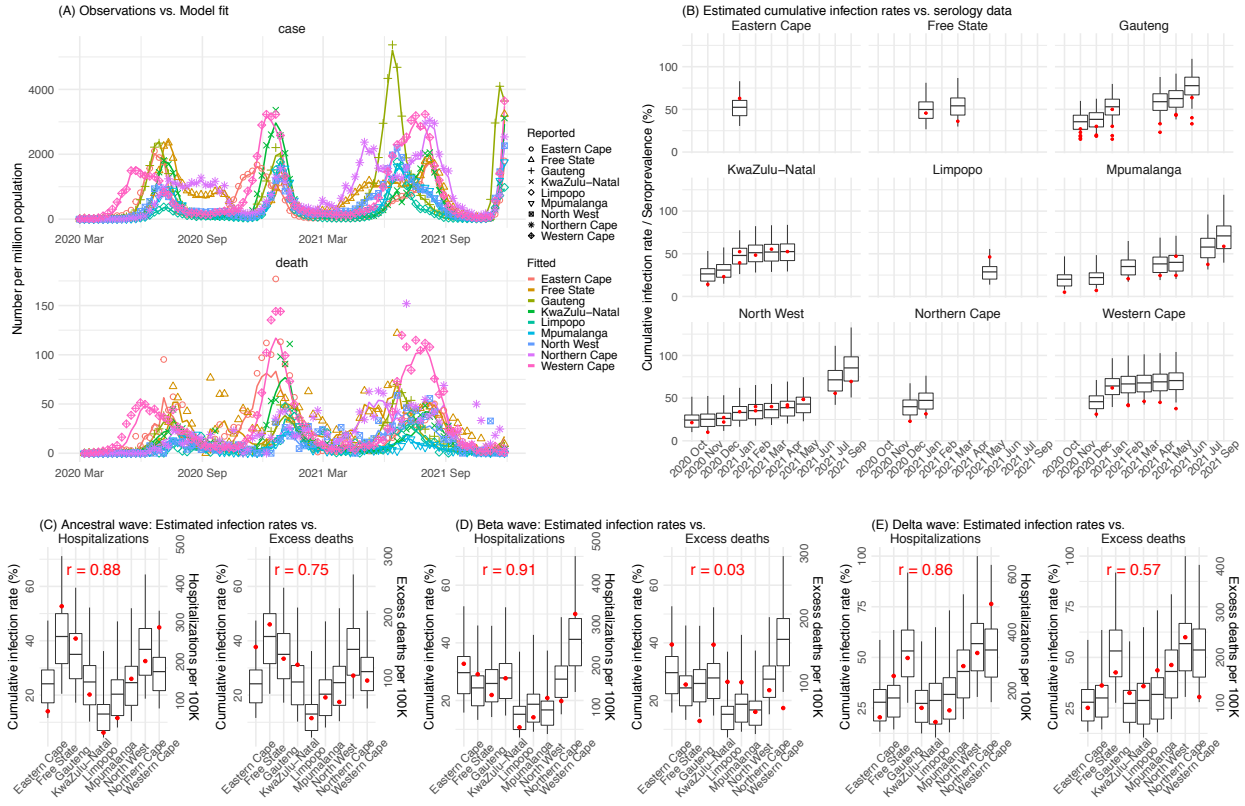

Fig 2. Example model-inference estimates for Gauteng. (A) Observed relative mobility, vaccination rate, and estimated disease seasonal trend, compared to case and death rates over time. Key model-inference estimates are shown for the time-varying effective reproduction number R_t (B), transmissibility (C), population susceptibility (D), infection-detection rate (E), and infection-fatality risk (F). Grey shaded areas indicate the approximate circulation period for each variant. In (B) – (F), blue lines and surrounding areas show the estimated mean, 50% (dark) and 95% (light) CrIs; boxes and whiskers show the estimated mean, 50% and 95% CrIs for estimated infection rates. *Note that the transmissibility estimates (in C) have removed the effects of changing population susceptibility, NPIs, and disease seasonality; thus, the trends are more stable than the reproduction number (R_t in B) and reflect changes in variant-specific properties. Also note that infection-fatality risk estimates were based on reported COVID-19 deaths and may not reflect true values due to likely under-reporting of COVID-19 deaths.*

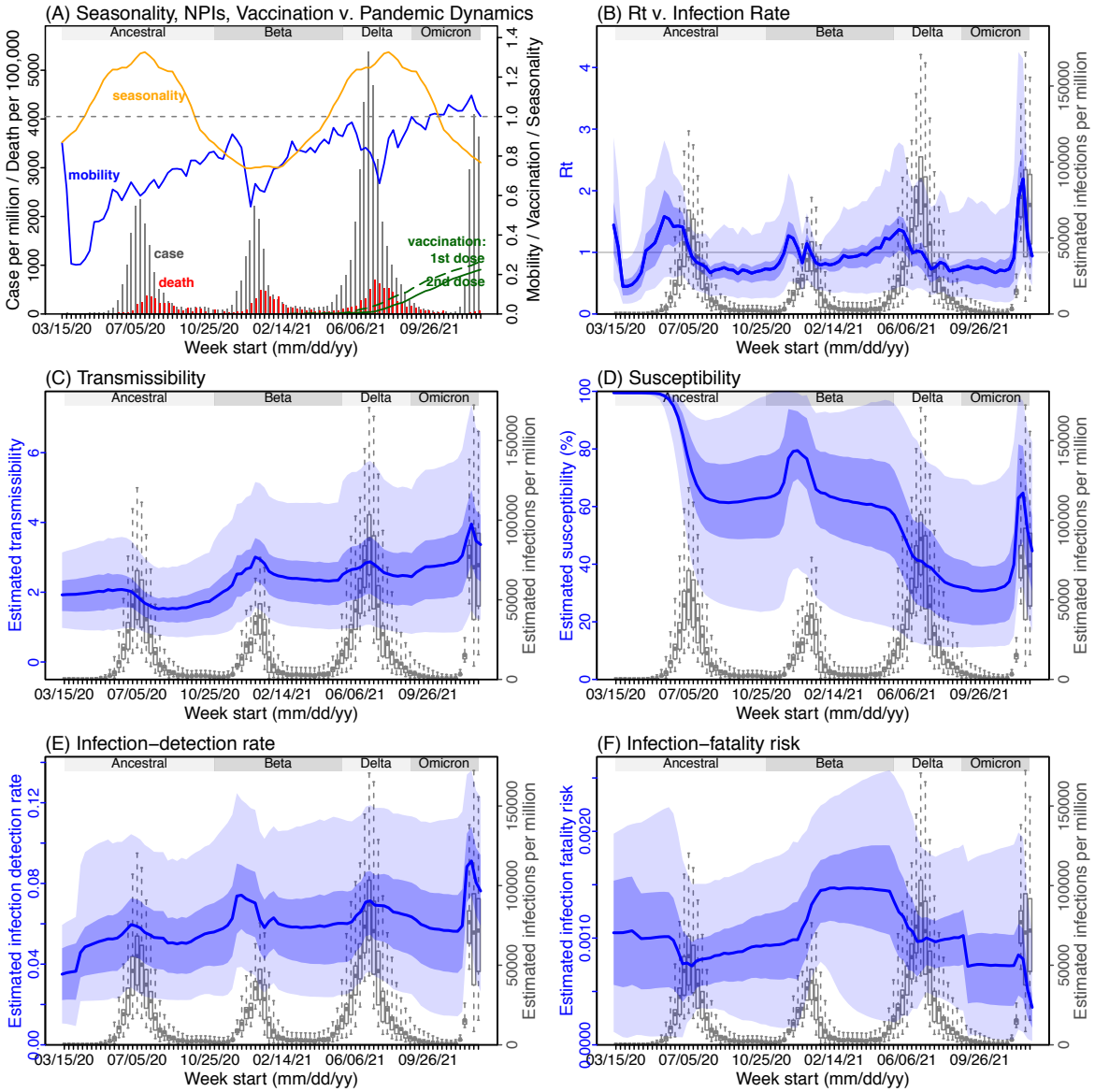

Fig 3. Model-inferred epidemiological properties for different variants across SA provinces. Heatmaps show (A) Estimated mean infection rates by week (x-axis) and province (y-axis), (B) Estimated mean *cumulative* infection numbers relative to the population size in each province, and (C) Estimated population susceptibility (to the circulating variant) by week and province. (D) Boxplots in the top row show the estimated distribution of changes in transmissibility for Beta, Delta, and Omicron, relative to the Ancestral SARS-CoV-2, for each province (middle bar = median; edges = 50% CIs; and whiskers =95% CIs); boxplots in the bottom row show, for each variant, the estimated distribution of immune erosion to all adaptive immunity gained from infection and vaccination prior to that variant. Red lines show the mean across all provinces. Estimates for Omicron are not shown for some provinces, as data were not sufficient for model inference.

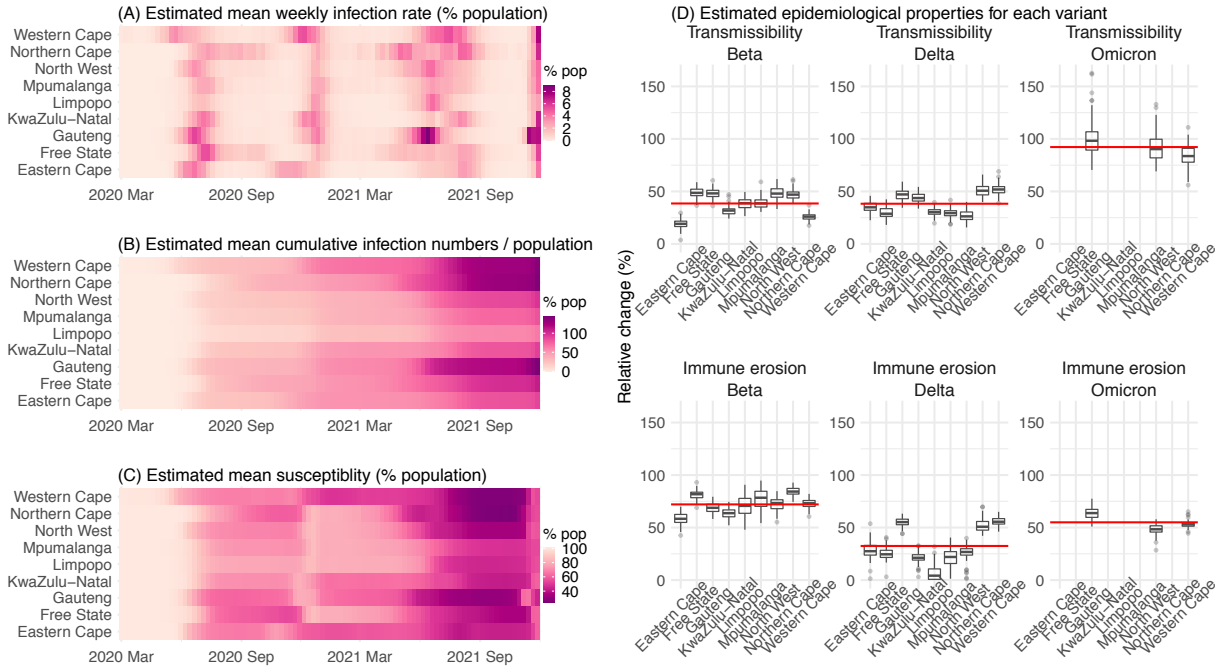

Supplemental Figures and Tables

Fig S1. Model-fit to case and death data in each province. Dots show reported SARS-CoV-2 cases and deaths by week. Blue lines and surrounding area show model estimated median, 50% (darker blue) and 95% (lighter blue) credible intervals.

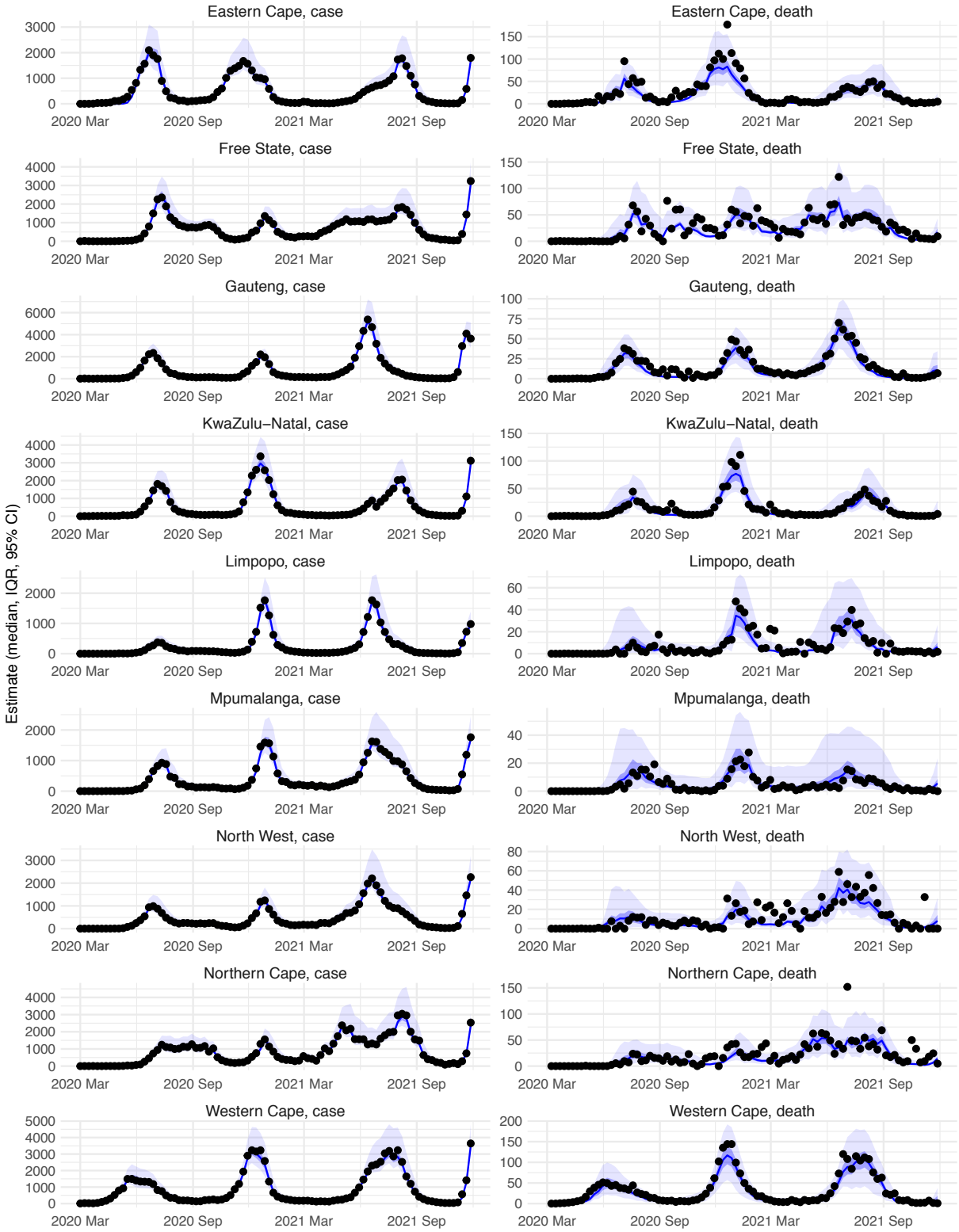

Fig S2. Model inference estimates for *Eastern Cape*. (A) Observed relative mobility, vaccination rate, and estimated disease seasonal trend, compared to case and death rates over time. Key model-inference estimates are shown for the time-varying effective reproduction number R_t (B), transmissibility (C), population susceptibility (D), infection-detection rate (E), and infection-fatality risk (F). Grey shaded areas indicate the approximate circulation period for each variant. In (B) – (F), blue lines and surrounding areas show the estimated mean, 50% (dark) and 95% (light) CrIs; boxes and whiskers show the estimated mean, 50% and 95% CrIs for estimated infection rates. *Note that the transmissibility estimates (in C) have removed the effects of changing population susceptibility, NPIs, and disease seasonality; thus, the trends are more stable than the reproduction number (R_t in B) and reflect changes in variant-specific properties. Also note that infection-fatality risk estimates were based on reported COVID-19 deaths and may not reflect true values due to likely under-reporting of COVID-19 deaths.*

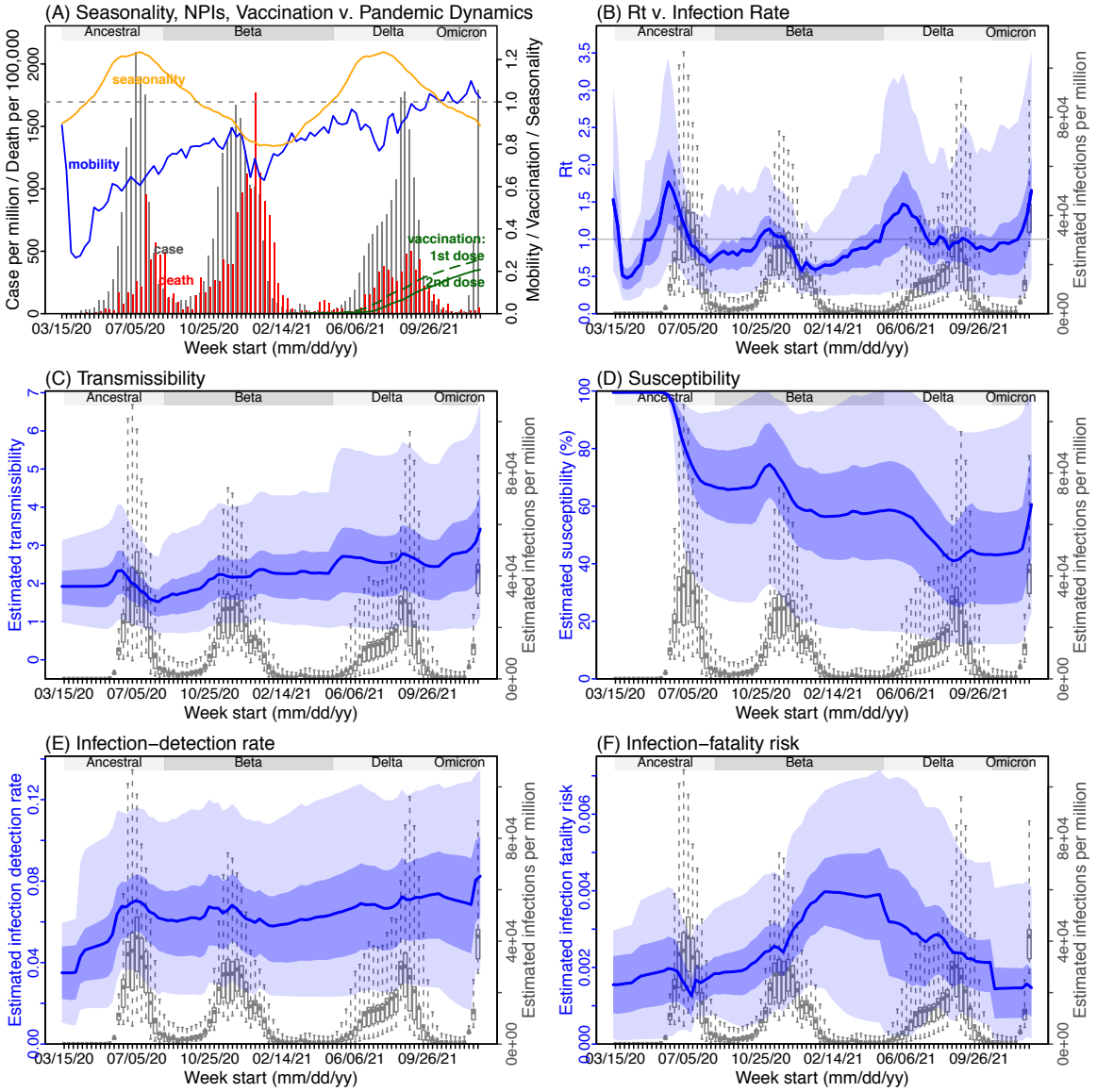

Fig S3. Model inference estimates for *Free State*. (A) Observed relative mobility, vaccination rate, and estimated disease seasonal trend, compared to case and death rates over time. Key model-inference estimates are shown for the time-varying effective reproduction number R_t (B), transmissibility (C), population susceptibility (D), infection-detection rate (E), and infection-fatality risk (F). Grey shaded areas indicate the approximate circulation period for each variant. In (B) – (F), blue lines and surrounding areas show the estimated mean, 50% (dark) and 95% (light) CrIs; boxes and whiskers show the estimated mean, 50% and 95% CrIs for estimated infection rates. *Note that the transmissibility estimates (in C) have removed the effects of changing population susceptibility, NPIs, and disease seasonality; thus, the trends are more stable than the reproduction number (R_t in B) and reflect changes in variant-specific properties. Also note that infection-fatality risk estimates were based on reported COVID-19 deaths and may not reflect true values due to likely under-reporting of COVID-19 deaths.*

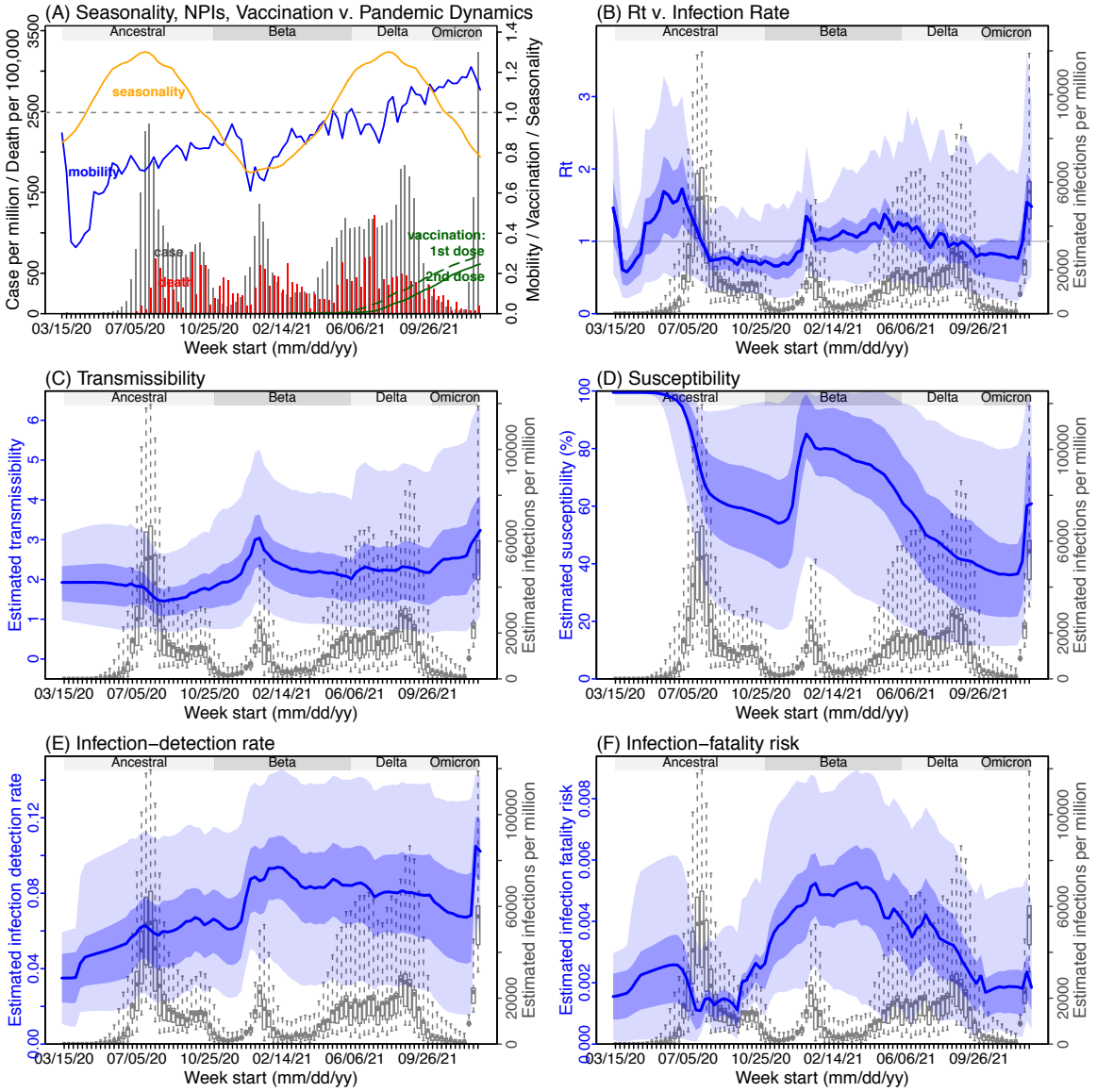

Fig S4. Model inference estimates for *KwaZulu-Natal*. (A) Observed relative mobility, vaccination rate, and estimated disease seasonal trend, compared to case and death rates over time. Key model-inference estimates are shown for the time-varying effective reproduction number R_t (B), transmissibility (C), population susceptibility (D), infection-detection rate (E), and infection-fatality risk (F). Grey shaded areas indicate the approximate circulation period for each variant. In (B) – (F), blue lines and surrounding areas show the estimated mean, 50% (dark) and 95% (light) CrIs; boxes and whiskers show the estimated mean, 50% and 95% CrIs for estimated infection rates. *Note that the transmissibility estimates (in C) have removed the effects of changing population susceptibility, NPIs, and disease seasonality; thus, the trends are more stable than the reproduction number (R_t in B) and reflect changes in variant-specific properties. Also note that infection-fatality risk estimates were based on reported COVID-19 deaths and may not reflect true values due to likely under-reporting of COVID-19 deaths.*

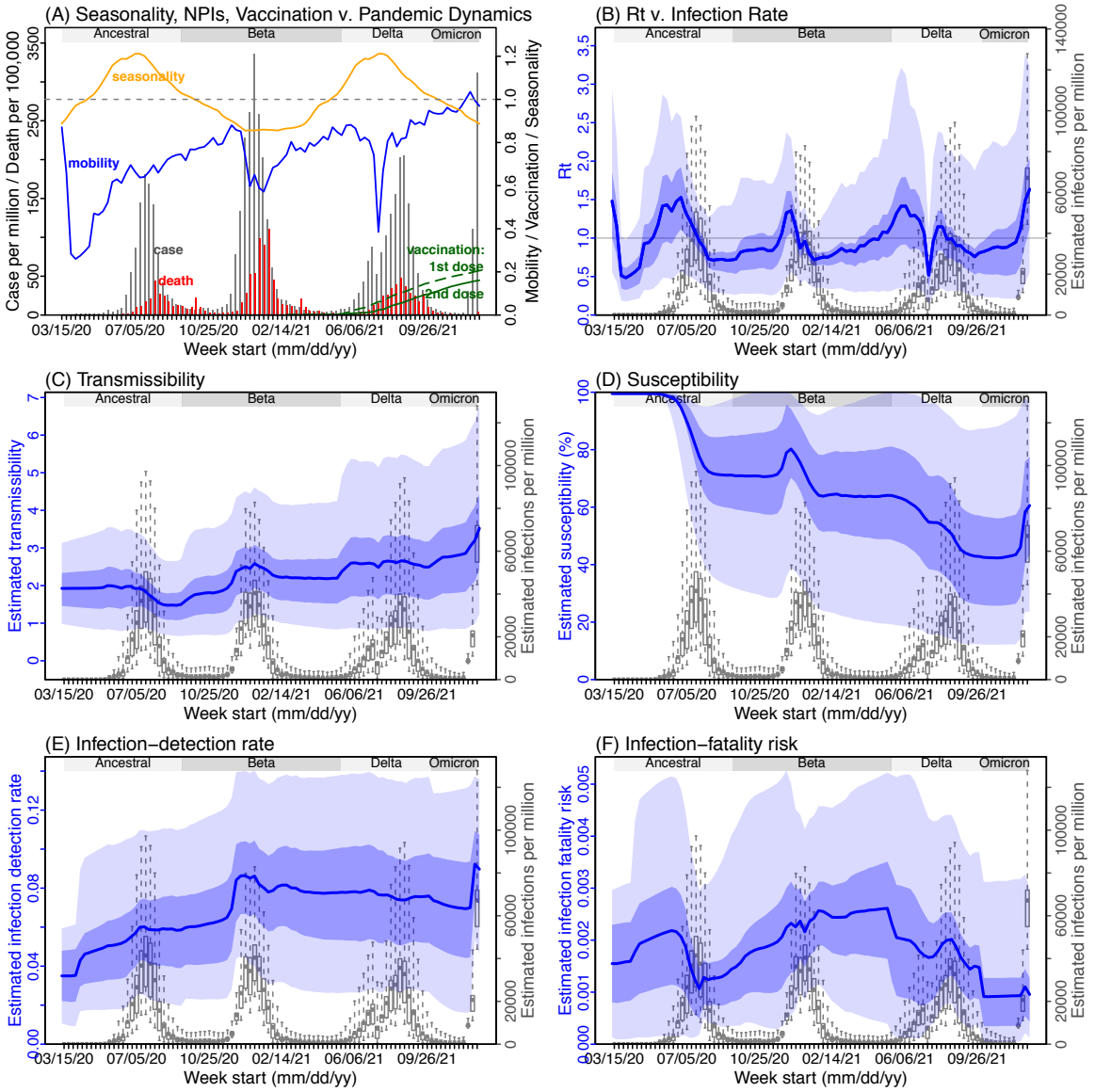

Fig S5. Model inference estimates for *Limpopo*. (A) Observed relative mobility, vaccination rate, and estimated disease seasonal trend, compared to case and death rates over time. Key model-inference estimates are shown for the time-varying effective reproduction number R_t (B), transmissibility (C), population susceptibility (D), infection-detection rate (E), and infection-fatality risk (F). Grey shaded areas indicate the approximate circulation period for each variant. In (B) – (F), blue lines and surrounding areas show the estimated mean, 50% (dark) and 95% (light) CrIs; boxes and whiskers show the estimated mean, 50% and 95% CrIs for estimated infection rates. *Note that the transmissibility estimates (in C) have removed the effects of changing population susceptibility, NPIs, and disease seasonality; thus, the trends are more stable than the reproduction number (R_t in B) and reflect changes in variant-specific properties. Also note that infection-fatality risk estimates were based on reported COVID-19 deaths and may not reflect true values due to likely under-reporting of COVID-19 deaths.*

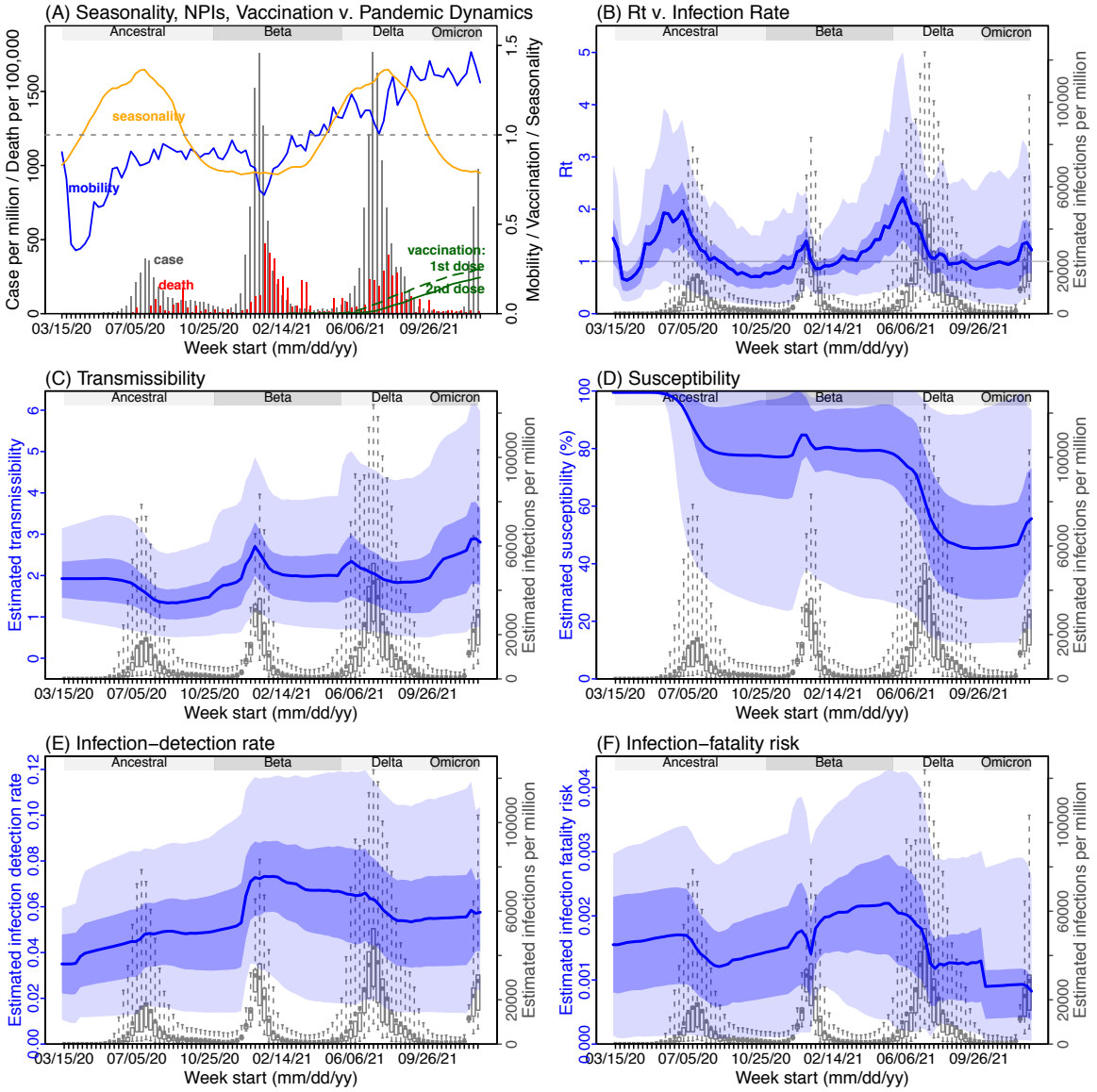

Fig S6. Model inference estimates for *Mpumalanga*. (A) Observed relative mobility, vaccination rate, and estimated disease seasonal trend, compared to case and death rates over time. Key model-inference estimates are shown for the time-varying effective reproduction number R_t (B), transmissibility (C), population susceptibility (D), infection-detection rate (E), and infection-fatality risk (F). Grey shaded areas indicate the approximate circulation period for each variant. In (B) – (F), blue lines and surrounding areas show the estimated mean, 50% (dark) and 95% (light) CrIs; boxes and whiskers show the estimated mean, 50% and 95% CrIs for estimated infection rates. *Note that the transmissibility estimates (in C) have removed the effects of changing population susceptibility, NPIs, and disease seasonality; thus, the trends are more stable than the reproduction number (R_t in B) and reflect changes in variant-specific properties. Also note that infection-fatality risk estimates were based on reported COVID-19 deaths and may not reflect true values due to likely under-reporting of COVID-19 deaths.*

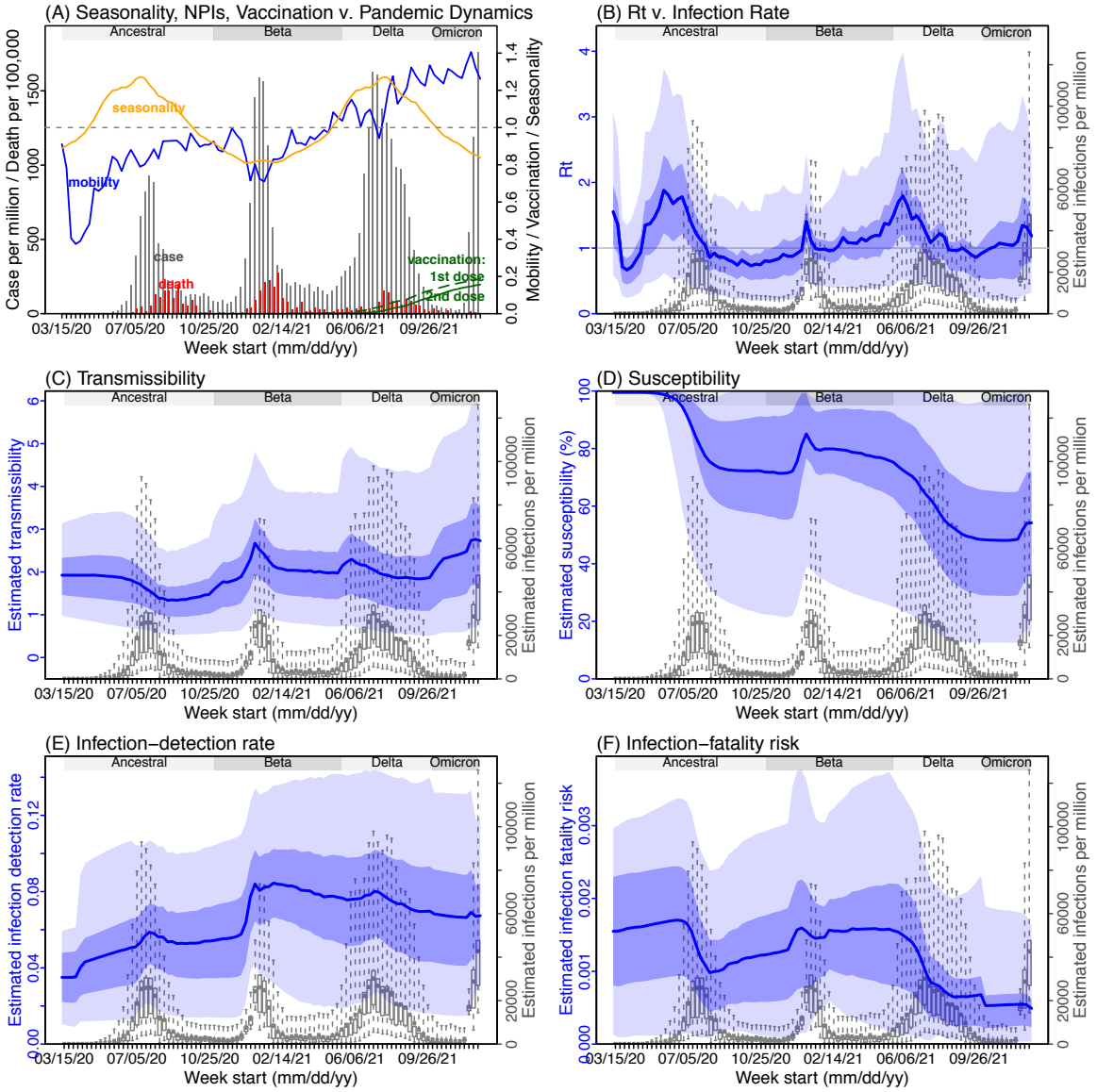

Fig S7. Model inference estimates for *North West*. (A) Observed relative mobility, vaccination rate, and estimated disease seasonal trend, compared to case and death rates over time. Key model-inference estimates are shown for the time-varying effective reproduction number R_t (B), transmissibility (C), population susceptibility (D), infection-detection rate (E), and infection-fatality risk (F). Grey shaded areas indicate the approximate circulation period for each variant. In (B) – (F), blue lines and surrounding areas show the estimated mean, 50% (dark) and 95% (light) CrIs; boxes and whiskers show the estimated mean, 50% and 95% CrIs for estimated infection rates. *Note that the transmissibility estimates (in C) have removed the effects of changing population susceptibility, NPIs, and disease seasonality; thus, the trends are more stable than the reproduction number (R_t in B) and reflect changes in variant-specific properties. Also note that infection-fatality risk estimates were based on reported COVID-19 deaths and may not reflect true values due to likely under-reporting of COVID-19 deaths.*

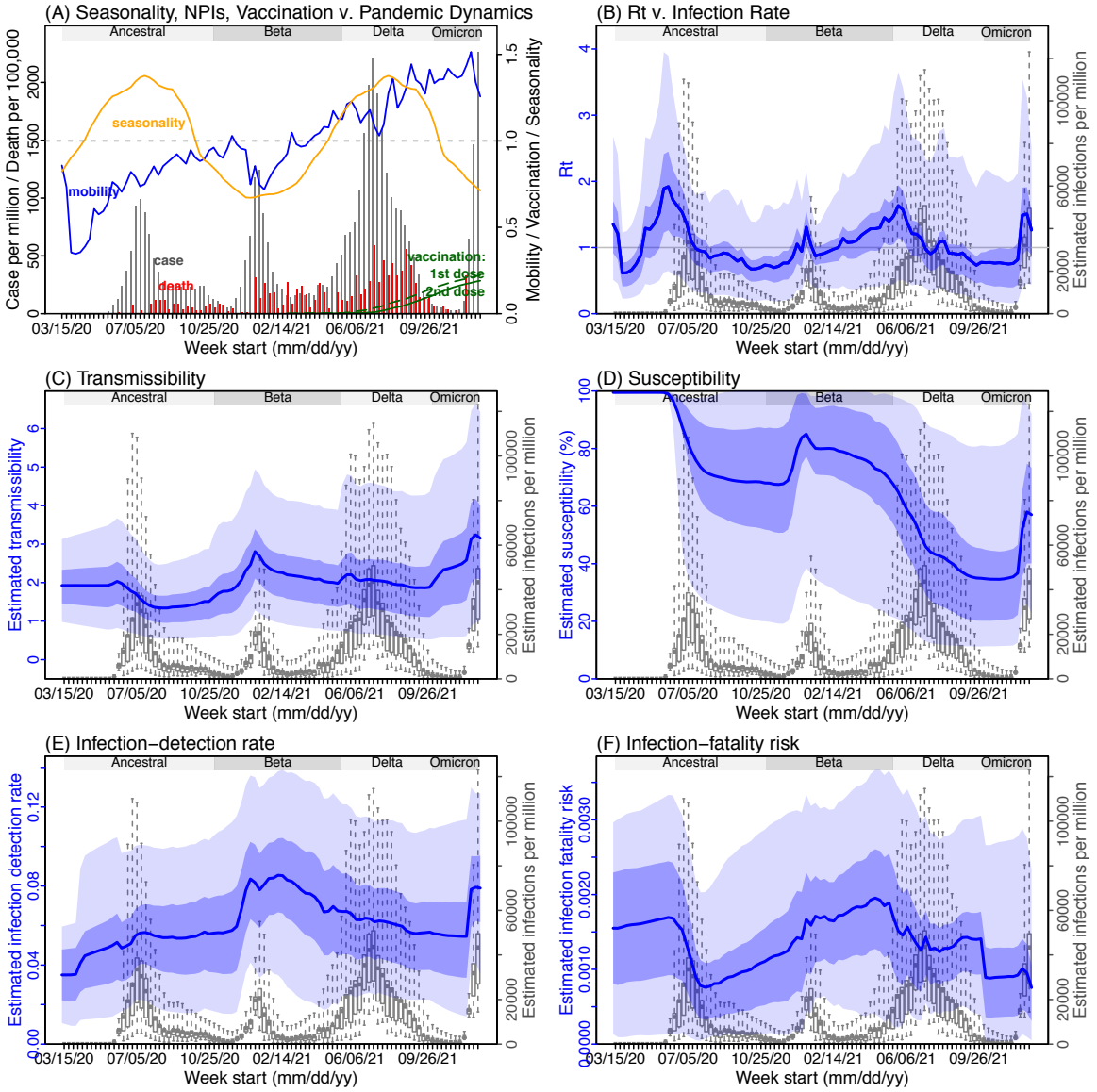

Fig S8. Model inference estimates for *Northern Cape*. (A) Observed relative mobility, vaccination rate, and estimated disease seasonal trend, compared to case and death rates over time. Key model-inference estimates are shown for the time-varying effective reproduction number R_t (B), transmissibility (C), population susceptibility (D), infection-detection rate (E), and infection-fatality risk (F). Grey shaded areas indicate the approximate circulation period for each variant. In (B) – (F), blue lines and surrounding areas show the estimated mean, 50% (dark) and 95% (light) CrIs; boxes and whiskers show the estimated mean, 50% and 95% CrIs for estimated infection rates. *Note that the transmissibility estimates (in C) have removed the effects of changing population susceptibility, NPIs, and disease seasonality; thus, the trends are more stable than the reproduction number (R_t in B) and reflect changes in variant-specific properties. Also note that infection-fatality risk estimates were based on reported COVID-19 deaths and may not reflect true values due to likely under-reporting of COVID-19 deaths.*

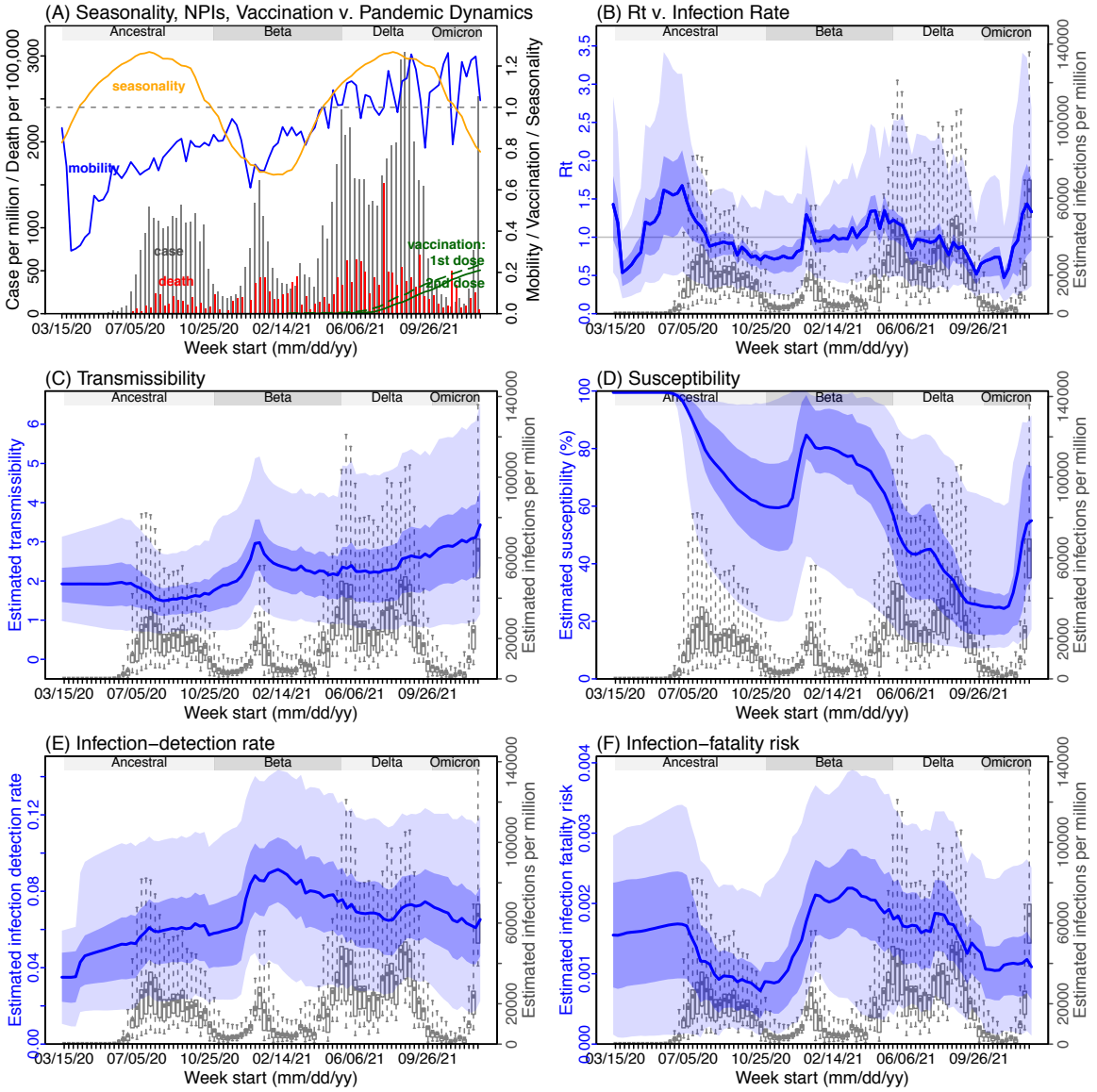

Fig S9. Model inference estimates for *Western Cape*. (A) Observed relative mobility, vaccination rate, and estimated disease seasonal trend, compared to case and death rates over time. Key model-inference estimates are shown for the time-varying effective reproduction number R_t (B), transmissibility (C), population susceptibility (D), infection-detection rate (E), and infection-fatality risk (F). Grey shaded areas indicate the approximate circulation period for each variant. In (B) – (F), blue lines and surrounding areas show the estimated mean, 50% (dark) and 95% (light) CrIs; boxes and whiskers show the estimated mean, 50% and 95% CrIs for estimated infection rates. *Note that the transmissibility estimates (in C) have removed the effects of changing population susceptibility, NPIs, and disease seasonality; thus, the trends are more stable than the reproduction number (R_t in B) and reflect changes in variant-specific properties. Also note that infection-fatality risk estimates were based on reported COVID-19 deaths and may not reflect true values due to likely under-reporting of COVID-19 deaths.*

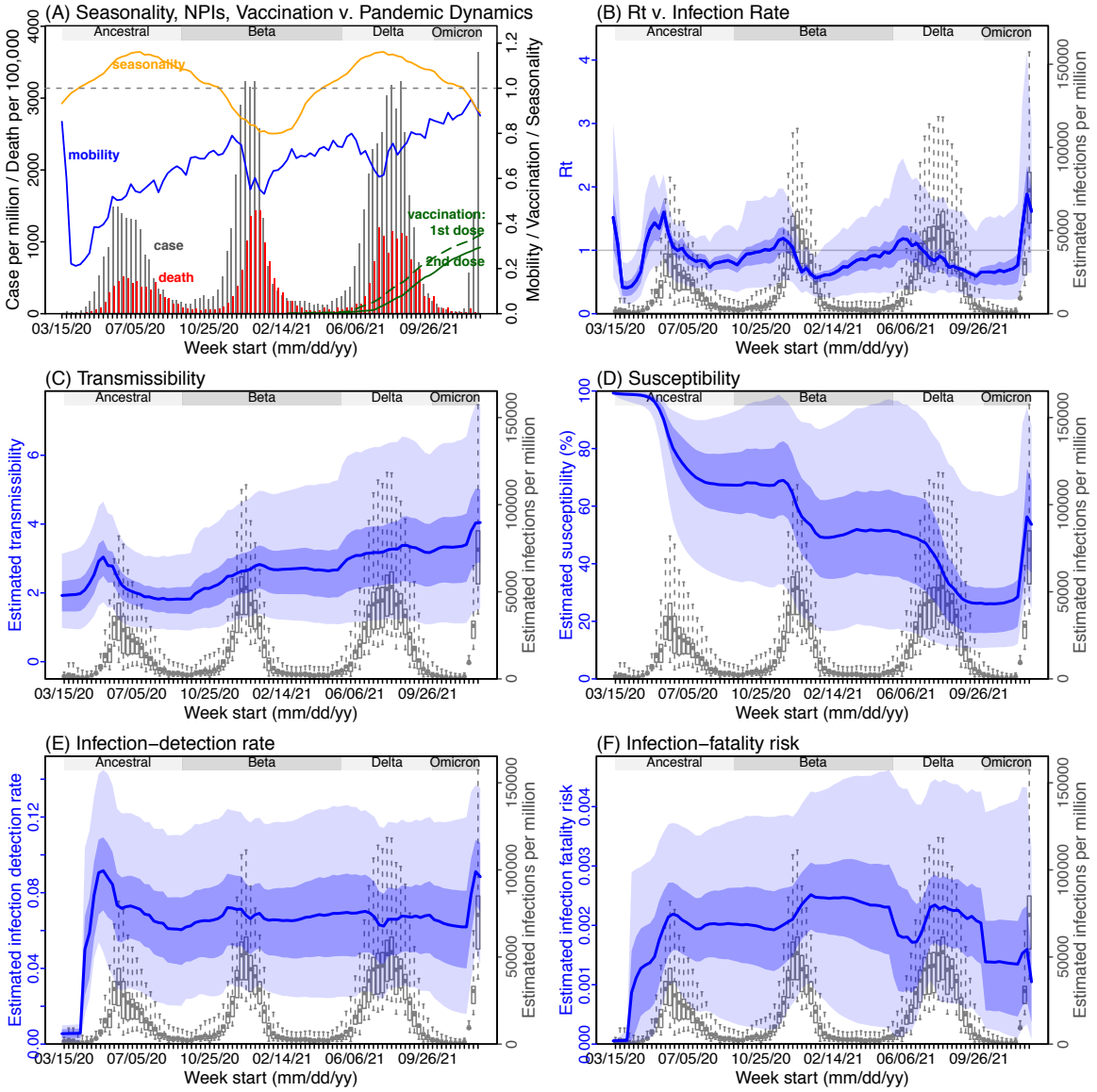

Table S1. Model estimated infection-detection rate during each wave. Numbers show the estimated percentage of infections (including asymptomatic and subclinical infections) documented as cases (mean and 95% CI in parentheses).

Province	Ancestral wave	Beta wave	Delta wave
Eastern Cape	5.16 (2.63, 10.74)	5.65 (3.18, 10.6)	5.12 (2.43, 10.69)
Free State	4.74 (2.77, 9.62)	6.65 (3.52, 12.2)	6.69 (3.16, 13.86)
Gauteng	4.31 (2.53, 8.75)	5.21 (2.94, 9.47)	5.88 (3.4, 11.32)
KwaZulu-Natal	4.19 (1.99, 10.16)	7.01 (3.73, 13.21)	5.66 (2.67, 12.39)
Limpopo	2.26 (0.81, 6.69)	5.15 (2.12, 10.94)	3.34 (1.48, 9.18)
Mpumalanga	3.19 (1.38, 8.04)	5.82 (2.54, 11.88)	4.89 (2.12, 11.91)
North West	3.37 (1.59, 7.96)	5.55 (2.49, 11.11)	4.55 (2.41, 10.01)
Northern Cape	4.71 (2.69, 9.28)	6.38 (3.58, 11.5)	6.54 (3.67, 12.19)
Western Cape	5.58 (3.13, 10.59)	6.39 (3.76, 11.47)	6.01 (3.37, 11.56)

Table S2. Model estimated attack rate during each wave. Numbers show estimated cumulative infection numbers, expressed as percentage of population size (mean and 95% CI in parentheses).

Province	Ancestral wave	Beta wave	Delta wave
Eastern Cape	24.17 (11.61, 47.43)	29.66 (15.81, 52.7)	27.88 (13.36, 58.64)
Free State	41.57 (20.5, 71.16)	24.37 (13.29, 46.02)	30 (14.47, 63.54)
Gauteng	34.99 (17.22, 59.52)	25.91 (14.26, 45.91)	53.19 (27.61, 91.87)
KwaZulu-Natal	24.84 (10.25, 52.22)	27.83 (14.78, 52.35)	27.3 (12.47, 57.92)
Limpopo	13.03 (4.39, 36.21)	15.21 (7.15, 36.94)	28.77 (10.47, 64.91)
Mpumalanga	20.34 (8.08, 47.13)	18.7 (9.16, 42.77)	31.74 (13.02, 73.22)
North West	24.59 (10.39, 51.98)	16.73 (8.37, 37.32)	43.06 (19.56, 81.15)
Northern Cape	36.83 (18.69, 64.41)	27.41 (15.22, 48.93)	56.81 (30.5, 101.16)
Western Cape	28.64 (15.09, 51.06)	41.21 (22.96, 70.11)	53.67 (27.93, 95.67)

Table S3. Model estimated infection-fatality risk during each wave. Numbers are percentages (%; mean and 95% CI in parentheses). Note that these estimates were based on reported COVID-19 deaths and may be biased due to likely under-reporting of COVID-19 deaths.

Province	Ancestral wave	Beta wave	Delta wave
Eastern Cape	0.15 (0.08, 0.31)	0.46 (0.26, 0.86)	0.19 (0.09, 0.39)
Free State	0.13 (0.07, 0.25)	0.42 (0.22, 0.76)	0.27 (0.13, 0.55)
Gauteng	0.09 (0.05, 0.18)	0.16 (0.09, 0.28)	0.1 (0.06, 0.19)
KwaZulu-Natal	0.09 (0.04, 0.22)	0.25 (0.13, 0.47)	0.14 (0.06, 0.3)
Limpopo	0.06 (0.02, 0.17)	0.21 (0.08, 0.44)	0.1 (0.04, 0.27)
Mpumalanga	0.06 (0.03, 0.16)	0.09 (0.04, 0.19)	0.04 (0.02, 0.09)
North West	0.05 (0.02, 0.11)	0.2 (0.09, 0.4)	0.14 (0.07, 0.3)
Northern Cape	0.06 (0.03, 0.11)	0.21 (0.12, 0.37)	0.17 (0.09, 0.31)
Western Cape	0.21 (0.12, 0.4)	0.27 (0.16, 0.48)	0.22 (0.12, 0.42)

Table S4. Prior ranges for the parameters used in the model-inference system.

Parameter/ variable	Symbol	Prior range	Source/rationale
Initial exposed	*E*(t=0)	1 – 100 times of reported cases during the Week of March 15, 2020 for Western Cape; 1 – 10 times of reported cases during the Week of March 15, 2020, for other provinces	Low infection-detection rate in first weeks; earlier and higher case numbers reported in Western Cape than other provinces.
Initial infectious	*I*(t=0)	Same as for *E*(t=0)	
Initial susceptible	*S*(t=0)	99 – 100% of the population	Almost everyone is susceptible initially
Population size	*N*	N/A	Based on population data from COVID19ZA (main text ref 24)
Variant-specific transmission rate	β	For all provinces, starting from U[0.4, 0.7] at time 0 and allowed to increase over time using space re-probing[5] with values drawn from U[0.5, 0.9] during the Beta wave, U[0.7, 1.25] during the Delta wave, and U[0.7, 1.3] during the Omicron wave.	For the initial range at model initialization, based on R_0 estimates of around 1.5-4 for SARS-CoV-2.[1-3] For the Beta, Delta and Omicron variants, we use large bounds for space re-probing (SR)[5] to explore the parameter state space and enable estimation of changes in transmissibility due to the new variants. Note that SR is only applied to 3-10% of the ensemble members and β can migrate outside either the initial range or the SR ranges during EAKF update.
Scaling of effectiveness of NPI	*e*	[0.5, 1.5], for all provinces	Around 1, with a large bound to be flexible.

Latency period	*Z*	[2, 5] days, for all provinces	Incubation period: 5.2 days (95% CI: 4.1, 7)[1]; latency period is likely shorter than the incubation period
Infectious period	*D*	[2, 5] days, for all provinces	Time from symptom onset to hospitalization: 3.8 days (95% CI: 0, 12.0) in China,[4] plus 1-2 days viral shedding before symptom onset. We did not distinguish symptomatic/asymptomatic infections.
Immunity period	*L*	[730, 1095] days, for all provinces	Assuming immunity lasts for 2-3 years
Mean of time from viral shedding to diagnosis	T_m	[5, 8] days, for all provinces	From a few days to a week from symptom onset to diagnosis/reporting,[4] plus 1-2 days of viral shedding (being infectious) before symptom onset.
Standard deviation (SD) of time from viral shedding to diagnosis	T_{sd}	[1, 3] days, for all provinces	To allow variation in time to diagnosis/reporting
Infection-detection rate	*r*	For Western Cape: starting from U[0.001, 0.01] at time 0 and allowed to increase over time using space re-probing[5] with values drawn from U[0.02, 0.1] during 4/19/- 9/15/20 (Ancestral wave), U[0.02, 0.12] during the Beta wave (9/16/20 – 5/15/21), U[0.03, 0.12] during the Delta wave	Large uncertainties; therefore, in general we use large prior bounds and large bounds for space re-probing (SR). Note that SR is only applied to 3-10% of the ensemble members and *r* can migrate

	(5/16/21 – 9/30/21), and U[0.01, 0.08] starting 10/1/21 (Omicron wave). For Limpopo and Mpumalanga: starting from U[0.01, 0.06] at time 0 and allowed to increase over time using space re-probing[5] with values drawn from U[0.01, 0.08] for Limpopo and U[0.01, 0.1] for Mpumalanga during 4/12/2020 - 10/31/20 (Ancestral wave), U[0.01, 0.1] during the Beta wave (11/1/20 – 5/15/21), U[0.01, 0.1] during the Delta wave (5/16/21 – 9/30/21), and U[0.01, 0.08] starting 10/1/21 (Omicron wave). For Other provinces: starting from U[0.01, 0.06] at time 0 and allowed to increase over time using space re-probing[5] with values drawn from U[0.02, 0.1] starting 4/12/2020 for the rest of Ancestral wave, U[0.02, 0.12] during the Beta wave, U[0.03, 0.12] during the Delta wave, and U[0.01, 0.08] starting 10/1/21 (Omicron wave).	outside either the initial range or the SR ranges during EAKF update. Western Cape had earlier and higher case numbers during March – April 2020 than other provinces, suggesting lower detection rate at the time. Lower case rates in Limpopo and Mpumalanga, suggesting likely lower detection rate; thus, we used slightly lower numbers for space-reprobing in these two provinces
Infection fatality risk (IFR)	For Western Cape: starting from U[0.00001, 0.0001] at time 0 and allowed to change over time using space re-probing[5] with values drawn from U[0.00001, 0.0003] during 3/16/20 – 4/11/20, U[0.00001, 0.003] during 4/12/20 – 5/15/21 (Ancestral wave and Beta wave), U[0.00001, 0.0015] during 5/16/21 – 9/30/21 (Delta wave) and U[0.00001, 0.00075] starting 10/1/21 (Omicron wave). For Gauteng: starting from [0.0001, 0.002] at time 0 and allowed to change over time using space re-probing[5] with values drawn from U[0.0001, 0.0015] during 4/19/2020 - 12/12/2020, values drawn from U[0.0001, 0.002] during 12/13/2020 – 5/15/21 (due to Beta), U[0.0001, 0.0015] during the Delta wave, and U[0.00001, 0.00075] starting 9/1/21 (Omicron wave).	Based on previous estimates[6] but extend to have wider ranges. Note that SR is only applied to 3-10% of the ensemble members and IFR can migrate outside either the initial range or the SR ranges during EAKF update. Western Cape had earlier and higher case numbers during March – April 2020 than other provinces, suggesting lower detection rate at the time. Initial mortality rate in Gauteng was relatively low because initial infections occurred mainly among middle-aged, returning holiday makers.[7]

	For Limpopo and Mpumalanga: starting from U[0.0001, 0.003] at time 0 and allowed to change over time using space re-probing[5] with values drawn from U[0.0001, 0.004] during the Beta wave, U[0.0001, 0.003] during the Delta wave, U[0.00001, .001] for Limpopo and U[0.00001, 0.00075] for Mpumalanga starting 10/1/21 (Omicron wave). For Eastern Cape: starting from U[0.0001, 0.003] at time 0 and allowed to change over time using space re-probing[5] with values drawn from U[0.0001, 0.004] during 4/19/20 – 12/1/20 (Ancestral wave and earlier phase of Beta wave), U[0.0001, 0.006] during 12/2/20 – 4/30/21 (the Beta wave), [0.0001, 0.003] during the Delta wave, and U[0.00001, 0.0015] or starting 10/16/21 (Omicron wave). For KwaZulu-Natal: starting from U[0.0001, 0.003] at time 0 and allowed to change over time using space re-probing[5] with values drawn from U[0.0001, 0.005] during 4/19/20 – 5/15/21 (ancestral wave and Beta wave), U[0.0001, 0.0015] during the Delta wave, and U[0.00001, 0.00075] starting 10/1/21 (Omicron wave). For Northern Cape: starting from U[0.0001, 0.003] at time 0 and allowed to change over time using space re-probing[5] with values drawn from U[0.00001, 0.0015] starting 10/1/21 (Omicron wave). For Free State: starting from U[0.0001, 0.003] at time 0 and allowed to change over time using space re-probing[5] with values drawn from U[0.0001, 0.006] during 3/16/20 – 10/31/20, U[0.0001, 0.008] during the Beta and Delta waves, and U[0.00001, 0.0015] starting 10/1/21 (Omicron wave).	Earlier spread of Beta in Eastern Cape, KwaZulu-Natal, and Northern Cape, higher numbers of deaths per capita reported. Free State reported higher number of deaths per capita.

References including in Table S4:

1 Li, Q. *et al.* Early Transmission Dynamics in Wuhan, China, of Novel Coronavirus–Infected Pneumonia. *New Engl J Med*, doi:10.1056/NEJMoa2001316 (2020).

2 Wu, J. T., Leung, K. & Leung, G. M. Nowcasting and forecasting the potential domestic and international spread of the 2019-nCoV outbreak originating in Wuhan, China: a modelling study. *Lancet*, doi:10.1016/S0140-6736(20)30260-9 (2020).

3 Li, R. *et al.* Substantial undocumented infection facilitates the rapid dissemination of novel coronavirus (SARS-CoV-2). *Science* **368**, 489-493, doi:10.1126/science.abb3221 (2020).

4 Zhang, J. *et al.* Evolving epidemiology and transmission dynamics of coronavirus disease 2019 outside Hubei province, China: a descriptive and modelling study. *The Lancet. Infectious diseases*, doi:10.1016/S1473-3099(20)30230-9 (2020).

5 Yang, W. & Shaman, J. A simple modification for improving inference of non-linear dynamical systems. *arXiv*, 1403.6804 (2014).

6 Verity, R. *et al.* Estimates of the severity of coronavirus disease 2019: a model-based analysis. *The Lancet. Infectious diseases*, doi:10.1016/S1473-3099(20)30243-7 (2020).

7 Giandhari, J. *et al.* Early transmission of SARS-CoV-2 in South Africa: An epidemiological and phylogenetic report. *Int J Infect Dis* **103**, 234-241, doi:10.1016/j.ijid.2020.11.128 (2021).

Table S5. Approximate epidemic timing for each wave in each province.

Province	Variant	Start date	End date
Eastern Cape	Ancestral	3/15/20	8/15/20
Eastern Cape	Beta	8/16/20	4/30/21
Eastern Cape	Delta	5/1/21	10/15/21
Eastern Cape	Omicron	10/16/21	NA
Free State	Ancestral	3/15/20	10/31/20
Free State	Beta	11/1/20	5/31/21
Free State	Delta	6/1/21	9/30/21
Free State	Omicron	10/1/21	NA
Gauteng	Ancestral	3/15/20	10/31/20
Gauteng	Beta	11/1/20	5/15/21
Gauteng	Delta	5/16/21	8/31/21
Gauteng	Omicron	9/1/21	NA
KwaZulu-Natal	Ancestral	3/15/20	9/15/20
KwaZulu-Natal	Beta	9/16/20	5/15/21
KwaZulu-Natal	Delta	5/16/21	9/30/21
KwaZulu-Natal	Omicron	10/1/21	NA
Limpopo	Ancestral	3/15/20	10/31/20
Limpopo	Beta	11/1/20	5/15/21
Limpopo	Delta	5/16/21	9/30/21
Limpopo	Omicron	10/1/21	NA
Mpumalanga	Ancestral	3/15/20	10/31/20
Mpumalanga	Beta	11/1/20	5/15/21
Mpumalanga	Delta	5/16/21	9/30/21
Mpumalanga	Omicron	10/1/21	NA
North West	Ancestral	3/15/20	10/31/20
North West	Beta	11/1/20	5/15/21
North West	Delta	5/16/21	9/30/21
North West	Omicron	10/1/21	NA
Northern Cape	Ancestral	3/15/20	10/31/20
Northern Cape	Beta	11/1/20	5/15/21
Northern Cape	Delta	5/16/21	9/30/21
Northern Cape	Omicron	10/1/21	NA
Western Cape	Ancestral	3/15/20	9/15/20
Western Cape	Beta	9/16/20	5/15/21
Western Cape	Delta	5/16/21	9/30/21
Western Cape	Omicron	10/1/21	NA